

July 21, 1997

MC-TH-97/12

FROM DEEP INELASTIC SCATTERING TO PHOTOPRODUCTION: A UNIFIED APPROACH

G. Kerley and G. Shaw

Department of Physics and Astronomy, Schuster Laboratory
University of Manchester, Manchester M13 9PL, U.K.

ABSTRACT

The strikingly different high energy behaviours of real photoabsorption cross-sections with $Q^2 = 0$ and the low x proton structure function at large Q^2 are studied from a laboratory frame viewpoint, in which the x and Q^2 dependence reflects the space-time structure of the interaction. This is done using a simple model which incorporates hadron dominance, but attributes the striking enhancement observed at HERA at very low x and high Q^2 to contributions from heavy long-lived fluctuations of the incoming photon. Earlier published predictions of the model for the then unknown behaviour of the structure function at small x and intermediate Q^2 are shown to be strikingly confirmed by recent experimental data. A simultaneous analysis of real photoabsorption data and structure function data for $0 \leq x < 0.1$ and $0 \leq Q^2 \leq 15 \text{ GeV}^2$ is then reported. An excellent fit is obtained, with all parameters in the restricted ranges allowed by other physical requirements.

1 Introduction

At high energies, the real photoabsorption cross-section

$$\sigma_{\gamma p}(\nu, Q^2 = 0) \approx a_P \nu^{\alpha_P - 1} + a_R \nu^{\alpha_R - 1}$$

is characterised by the intercept $\alpha_P \approx 1.08$ of the “soft” pomeron familiar from hadron scattering [1], together with an effective contribution from lower lying Regge trajectories with $\alpha_R \approx 0.55$. The same behaviour characterises the proton structure function in the intermediate x -region $0.02 \leq x \leq 0.1$, but experiments at HERA [2, 3] in 1993 first observed the much sharper rise in the structure function at small $x < 0.02$ and large $Q^2 > 8 \text{ GeV}^2$ associated with the “hard” pomeron. Here we focus on the transition between these contrasting behaviours in the intermediate Q^2 region $0 < Q^2 < 8 \text{ GeV}^2$ using an approach suggested by one of us [4]. This was used to predict the behaviour at intermediate Q^2 in 1994 [5], but there was no data with which to confront the predictions. Subsequently the experimental situation has been transformed by precise data both at high Q^2 and in the hitherto unexplored region of low x and intermediate Q^2 . [6, 7, 8]. Here we examine whether the new data at intermediate Q^2 agree with the prior predictions of the model; and whether its greater precision and its extension to smaller x -values enable the intercept of the hard pomeron to be determined more precisely by the data.

The model used is described in the next section. However it will be useful to first summarise the underlying approach [4]. This adopts the laboratory frame viewpoint typical of hadron dominance models, and emphasizes the role of the coherence length

$$l = \frac{2\nu}{m^2 + Q^2} = \frac{1}{Mx} \frac{1}{1 + m^2/Q^2} > \frac{1}{Mx}, \quad (1)$$

which represents the typical distance travelled by a vacuum fluctuation of the photon of mass m . Our assumptions on the nature of the dominant states at different coherent lengths are summarised in Figure 1. At short coherence lengths, $l < l_0 \approx 1 \text{ f}$, corresponding to large x values $x > 0.1$, we assume that these states are essentially bare $\bar{q}q$ pairs and a hadronic component of the photon has not developed. At moderate coherence lengths, they are assumed to have the single hadron-like behaviour expected for constituent $\bar{q}q$ pairs or vector mesons. However at very long coherence lengths, the photon fluctuations can eventually develop into the hadronic final states observed in e^+e^- annihilations¹. For low masses, these states can be approximated by a sum of vector mesons; but for high masses complicated jet-like final states are observed. The idea is that the new phenomena at very small x are associated with complicated jet-like states which only play a role for masses m and coherence lengths l which are greater than some critical values $m > m_J$ and $l > l_C$. By (1) this implies that they are confined to energies

$$\nu > \nu_C \equiv m_J^2 l_C / 2 \quad (Q^2 = 0) \quad (2)$$

¹For an attempt to understand the role of the coherence length from a more fundamental dynamical viewpoint, see Del Duca, Brodsky and Hoyer [9].

in photoproduction, and to the kinematic region

$$x < x_C(Q^2) \equiv \frac{1}{Ml_C} \frac{Q^2}{Q^2 + m_J^2} \quad (3)$$

for structure functions. The remaining states with $m < m_J$ and/or $l < l_C$ will completely dominate outside this region. They are included using conventional hadron dominance ideas which emphasize the link between real and virtual photons and provide a natural framework for describing the onset of scaling in the region² $x_C < x < 0.1$. For example, they give a good description of the transition between real photoabsorption and deep inelastic scattering data on protons in the intermediate x -region $0.02 \leq x \leq 0.1$ [4, 10]; and they successfully predict the observed shadowing behaviour for real photoabsorption and deep inelastic scattering on nuclei in the same x region [11, 12, 13].

2 A simple model

In the hadron dominance model³, the total cross-section for photoabsorption is given by an expression of the form

$$\sigma_{\gamma p}(\nu, Q^2) = \int dm^2 \int dm'^2 \frac{\rho(m, m', s)}{(m^2 + Q^2)(m'^2 + Q^2)} \quad (4)$$

corresponding to Figure 2. Conventional hadron physics and duality with the parton model both require large “diagonal” $m = m'$ and large “off-diagonal” $m \neq m'$ components to be present; and the latter must be explicitly incorporated if the approximate scaling behaviour of the shadowing for deep inelastic scattering on heavy nuclei is to be understood [11, 12, 13]. However, these off-diagonal contributions are dominated by terms in which the two mass values m and m' are not very different. Equation (4) is therefore often replaced by a simple diagonal approximation

$$\sigma_{\gamma p}(\nu, Q^2) = \int_{m_0^2}^{\infty} dm^2 \frac{\rho(\nu, m^2)}{(m^2 + Q^2)^2}, \quad (5)$$

where $\rho(\nu, m^2)$ is an effective quantity, meant to represent the more complicated structure on average⁴. Single hadron-like behaviour of the intermediate states can be incorporated by assuming a Regge-type energy dependence

$$\rho^P(\nu, m^2) = f_P(m^2) \nu^{\alpha_P - 1}$$

²In hadron dominance models which give approximate scaling, the bulk of the contributions for a given Q^2 comes from intermediate states with $0 < m^2 < n Q^2$, with n a small integer. The average value is of order $m^2 \approx Q^2$, for which the coherence length $l \approx 1/2Mx$ by (1).

³For reviews, see for example [4] and [14] and references therein.

⁴If (5) were exact, in the context of scaling in $e^+ e^-$ annihilation and deep inelastic scattering it would imply that the total cross-sections σ_m for states m scattering on nucleons decreased approximately as m^{-2} . This counter-intuitive result is sometimes known as the Gribov paradox. It implies that the mean free paths in nuclear matter increase like m^2 , so that shadowing would die away at large Q^2 at fixed x . These problems do not occur in “off-diagonal models” of the form (5), when the effective quantity $\rho(\nu, m^2)$ results from destructive interference between diagonal and off-diagonal terms in (4). (Again, see [4, 12, 14] and references therein.)

for the dominant diffractive contribution, where $f_P(m^2)$ is a smoothly varying function of mass chosen to lead to approximate scaling at large Q^2 . In particular, if we assume

$$\rho^P(\nu, m^2) = a\nu^{\alpha_P-1}(m^2)^{1-\alpha_P} \quad (6)$$

this gives

$$F_2^P = A x \nu^{\alpha_P} \int_{m_0^2}^{\infty} dm^2 \frac{(m^2)^{1-\alpha_P}}{(m^2 + Q^2)^2} \quad (7)$$

for the soft pomeron contribution to the structure function, where

$$A = \frac{M a}{2 \pi^2 \alpha}.$$

This formula obviously embodies single hadron-like behaviour $\alpha_P \approx 1.08$ for all intermediate states. Here we modify it by adjusting the contributions from $m > m_J$ and $l > l_C$, which is meant to roughly characterize the region in which single hadron-like behaviour has given way to a more complicated behaviour. This behaviour is unknown, so we parameterize it by the simplest possible generalization of (6), in which A , α_P are replaced by new parameters \tilde{A} , α'_P to allow for a different magnitude and energy dependence. In this way we arrive at a representation of the form

$$\begin{aligned} F_2^P = & \\ & Ax\nu^{\alpha_P} \int_{m_0^2}^{\infty} dm^2 \frac{(m^2)^{1-\alpha_P}}{(m^2 + Q^2)^2} [\theta(m_J^2 - m^2) + \theta(m^2 - m_J^2)\theta(l_C - l)] \\ & + \tilde{A}x\nu^{\alpha'_P} \int_{m_0^2}^{\infty} dm^2 \frac{(m^2)^{1-\alpha'_P}}{(m^2 + Q^2)^2} \theta(m^2 - m_J^2)\theta(l - l_C). \end{aligned} \quad (8)$$

For data fits, this is conveniently rewritten as

$$\begin{aligned} F_2^P = & \theta(m_C^2 - m_J^2) \left[Ax\nu^{\alpha_P} \int_{m_0^2}^{m_J^2} dm^2 \frac{(m^2)^{1-\alpha_P}}{(m^2 + Q^2)^2} \right. \\ & + \tilde{A}x\nu^{\alpha'_P} \int_{m_J^2}^{m_C^2} dm^2 \frac{(m^2)^{1-\alpha'_P}}{(m^2 + Q^2)^2} + Ax\nu^{\alpha_P} \int_{m_C^2}^{\infty} dm^2 \frac{(m^2)^{1-\alpha_P}}{(m^2 + Q^2)^2} \Big] \\ & + \theta(m_J^2 - m_C^2) \left[Ax\nu^{\alpha_P} \int_{m_0^2}^{\infty} dm^2 \frac{(m^2)^{1-\alpha_P}}{(m^2 + Q^2)^2} \right] \end{aligned} \quad (9)$$

where the integrals can conveniently approximated by rapidly convergent series, as shown in the Appendix, and the critical coherence length is replaced by an effective critical mass,

$$m_C^2(x, Q^2) \equiv Q^2 \left(\frac{1}{x M_p l_C} - 1 \right), \quad (10)$$

which, unlike m_J^2 (and l_C), depends on Q^2 and x . The real photon equivalent is

$$\begin{aligned} \sigma_{\gamma p}^P(\nu, 0) = & \theta(2\nu/l_C - m_J^2) \left[B\nu^{\alpha_P-1} \left((m_0^2)^{-\alpha_P} - (m_J^2)^{-\alpha_P} \right) \right. \\ & + C\nu^{\alpha'_P-1} \left((m_J^2)^{-\alpha'_P} - (2\nu/l_C)^{-\alpha'_P} \right) + B\nu^{\alpha_P-1} (2\nu/l_C)^{-\alpha_P} \Big] \\ & + \theta(m_J^2 - 2\nu/l_C) \left[B\nu^{\alpha_P-1} (m_0^2)^{-\alpha_P} \right] \end{aligned} \quad (11)$$

where

$$B \equiv \frac{2\pi^2\alpha}{2.568M_p}\frac{A}{\alpha_P}, \quad C \equiv \frac{2\pi^2\alpha}{2.568M_p}\frac{\tilde{A}}{\alpha'_P}. \quad (12)$$

and the numerical coefficients are chosen to give the cross section in mb for masses in GeV .

In addition to the contributions associated with the hard and soft pomerons, there is also an additional contribution associated with lower lying Regge poles. This is a small correction in the region we are considering, and we incorporate it using the simple empirical form

$$F_2^R(x, Q^2) = A_R x^{1-\alpha_R} \left(\frac{Q^2}{Q^2 + a_R} \right)^{\alpha_R}, \quad (13)$$

proposed by Donnachie and Landshoff [15], with the Regge intercept $\alpha_R = 0.55$. The total structure function is then given by

$$F_2(x, Q^2) = F_2^P + F_2^R. \quad (14)$$

In the “pre-HERA” regions $\nu < \nu_C$ ($Q^2 = 0$) and $x > x_C(Q^2)$, (9) reduces to the simpler form (7), and our parameterisation (14) can be made numerically almost identical to the empirical Donnachie and Landshoff parameterisation [15], which is known to give an excellent fit to photoproduction data and to structure function data in the intermediate region $0.1 > x > 0.01$. Correspondingly, data in this region effectively determines the parameters A, m_0, A_R and a_R in (9, 13). The additional parameters $\tilde{A}, \alpha'_P, m_J, l_C$ in (9) describe the behaviour at very small x , with m_J, l_C constrained to be a few GeV and a few fermi respectively.

3 Predictions at intermediate Q^2

In 1994 [5], the parameters A, m_0, A_R and a_R were fixed by fitting the simple representation (7, 13, 14)) to the “pre-HERA” data on real photoabsorption and the structure function at intermediate x values $0.02 < x < 0.1$. The additional parameters $\tilde{A}, \alpha'_P, m_J, l_C$ in the final form (9) were then determined by extending the fit to include the then recently available H1 data [16] at small x and large $Q^2 > 8 GeV^2$; and used to predict the behaviour at intermediate Q^2 ($0 < Q^2 < 8 GeV^2$), where no data existed. In particular, the dramatic rise at small x observed at high Q^2 was predicted to decrease rapidly and shift towards $x = 0$ as Q^2 becomes smaller. In this short section, we compare these predictions with the subsequent H1 measurements [6], in order to test the validity of the model⁵.

Before doing this, we consider the quality of the 1994 fits for $Q^2 > 8 GeV^2$. This is illustrated in Figure 3 for the Regge intercepts

$$\alpha_R = 0.55 \quad \alpha_P = 1.08, \quad (15)$$

⁵Since the 1994 fits were based on the 1993 H1 data at large Q^2 , we initially compare their predictions at lower Q^2 to later data from the same experiment. The data from ZEUS and other experiments will be discussed explicitly in the next section.

together with both a “conventional” value $\alpha'_P = 1.27$ and a very unconventional choice $\alpha'_P = 1.08$ for the intercept of the long-lived, high mass states associated with the hard pomeron in this approach. As can be seen, this intercept was not well determined by the existing data, because of the limited x -range covered. However the 1996 H1 data [6] are more precise and extend to smaller x -values. Plotting the same curves against this new data in Figure 4 leads to a clear preference for $\alpha'_P = 1.27$, although there are small discrepancies between the precise new data and the fit, since the parameters of the latter were determined by data of lower accuracy.

We now compare the 1994 predictions for the intermediate Q^2 region $0 < Q^2 < 8 \text{ GeV}^2$ with the 1996 H1 data, restricting ourselves to the case $\alpha'_P = 1.27$ in the light of the previous discussion⁶. Since in 1994 there was no data at all in this region that could be used to help determine the parameters of the fit, the curves shown in Figure 5 represent a genuine prediction. When taken in conjunction with Figure 4, they show that the Q^2 dependence predicted by the model is in excellent agreement with experiment.

4 A global analysis

In the last section we focussed upon the 1996 H1 data at small x and intermediate Q^2 because the parameters of the 1994 predictions were fixed by high Q^2 data from the 1994 H1 experiment. Here we report the results of a simultaneous chi-squared fit to all the recent photoabsorption data in the wider kinematic region $0 \leq x < 0.1$ and⁷ $0 \leq Q^2 \leq 15 \text{ GeV}^2$. In doing so, we allow all the parameters in the diffractive term (9), including the Regge intercepts α_P and α'_P , to be determined by photoabsorption alone, in order to see whether the resulting values accord with reasonable physical expectations. However, since the non-diffractive term (13) makes only a small contribution in this region, we keep the Regge intercept fixed at the value $\alpha_R = 0.55$ obtained from hadron scattering data, leaving A_R and a_R as variable parameters.

The data used in the fit comprise the small x data of the H1 [6], and ZEUS [7] collaborations; the small and intermediate x data of the E665 [8] collaboration; the intermediate- x data [17] of the NMC collaboration; and the real photoabsorption cross sections [18, 19, 20, 21, 22]. Obviously, we need to consider the consistency of the different experiments. The ZEUS and H1 data cover a similar kinematic region, and are consistent within errors, as we shall see. In addition, for $x \approx 0.01$ there is data from both E665 and NMC at low and intermediate Q^2 , as well as high Q^2 data from ZEUS and H1. As can be seen from Fig.6, the experiments are consistent with each other, except for the three NMC points at $(x, Q^2) = (0.0125, 3.26)$ $(0.0125, 4.52)$ and, especially, $(0.008, 3.47)$.

⁶For $3 \times 10^{-4} < x < 5 \times 10^{-3}$, the predictions are insensitive to the choice of α'_P , but outside this range the value 1.27 rather than 1.08 is preferred.

⁷We restrict ourselves to $Q^2 \leq 15 \text{ GeV}^2$ since we are interested in the transition region from real photons to deep inelastic behaviour. Our simple model will of course break down eventually, since it gives exact scaling as $Q^2 \rightarrow \infty$.

The resulting fits to the various data sets are shown in Figures 7-11 and the corresponding chi-squared contributions listed in Table 1, where in all cases, the statistical and point systematic errors have been combined in quadrature. As can be seen, good fits are obtained for all data sets with the possible exception of the NMC data, which contributes 94 towards chi-squared from 66 data points. However it is clear from Fig. 10 that the fit is satisfactory, except for a few points, usually towards the edge of the kinematic range of the experiment, which make a very large contribution to χ^2 . For example, the three NMC points discussed above contribute 23 towards chi-squared; and on examining Fig. 6, it is difficult to see how any smooth curve, which fits the rest of the data, can do any better.

With this small caveat, we conclude that the consistency of the data and the quality of the fit are very satisfactory. The corresponding parameter values are given in Table 2 together with their errors⁸. In addition, we have performed a series of seven fits in which one of the data sets listed in Table 1 is omitted, and the remaining six are fitted, in order check whether the parameter values are sensitive to small changes in the data set. The results are summarised in Table 3. As can be seen, the parameters are fairly stable against such changes, except for the parameters A_R , a_R associated with the small non-diffractive term (13). These are only separately well determined⁹ if the NMC data, covering the intermediate x -region, are included.

We now comment briefly on the values obtained for the parameters. In contrast to the 1994 fits, the intercept

$$\alpha'_P = 1.289 \pm 0.007 \quad (16)$$

of the hard pomeron is well determined, while the value

$$\alpha_P = 1.059 \pm 0.007$$

of the intercept of the soft pomeron is similar to, but perhaps slightly lower than, the value $\alpha_P = 1.08$ favoured by the analysis of hadronic total cross-sections [1] in terms of a simple Regge pole model of the pomeron. The value

$$m_0 = 0.68 \pm 0.01$$

is somewhat below the ρ mass, as predicted long ago by generalized vector dominance models with off-diagonal terms¹⁰, while the value of the parameter

$$m_J = 2.51 \pm 0.02$$

corresponding to the transition from resonance dominance to jet-like behaviour accords well with $e^+ e^-$ annihilation data. Finally the value for the characteristic distance over which jet-like behaviour develops for heavy states is

$$l_C = 3.45 \pm 0.06 \text{ fm}.$$

⁸These errors are, of course, correlated; the full error matrix is available on request.

⁹The ratio is well determined by real photoabsorption data.

¹⁰This follows naturally from the destructive interference between the diagonal and off-diagonal terms [14, 23].

This is also very reasonable, given the usual estimate $l \approx 1 \text{ fm}$ for the characteristic distance over which light $q\bar{q}$ states develop into vector mesons, based on, for example, the onset of nuclear shadowing effects in photoproduction on nuclei.

5 Summary

We have given a unified treatment of both real and virtual photoabsorption data in terms of a modified hadron dominance model, in which the striking enhancement observed at HERA at very low x and high Q^2 is attributed to contributions from heavy long-lived fluctuations of the incoming photon. We have shown:

- that the published predictions of the model for small x and low and intermediate $Q^2 < 8 \text{ GeV}^2$, where no data previously existed, are confirmed by recent data;
- that the model gives an excellent fit to the much improved real photoabsorption and proton structure function data over the whole region $0 \leq x < 0.1$ and $0 \leq Q^2 \leq 15 \text{ GeV}^2$;
- that the values of the parameters of the model, determined from this real and virtual photoabsorption data alone, are in good agreement with physical expectations and other sources of information.

6 Appendix: evaluation of integrals

Data fits were performed using the MINUIT routine to minimise chi-squared with respect to the parameters of equation (9). This is computationally quite involved and speed and efficiency are at a premium. For this reason the integrals in (9) were evaluated by using a convenient series expansion rather than the normal methods of numerical quadrature.

The integrals in (9) can be easily written as linear combinations of integrals of the form

$$\int_b^\infty \frac{z^{-\epsilon}}{(Q^2 + z)^2} dz \quad ; \quad 0 < |\epsilon| < 1 \quad (17)$$

where the lower limits usually arise from the step functions, and can depend on x and Q^2 . Writing $Q^2 y = z$,

$$\int_b^\infty \frac{z^{-\epsilon}}{(Q^2 + z)^2} dz = Q^{-2(1+\epsilon)} J(r, \epsilon) \quad (18)$$

where

$$J(r, \epsilon) = \int_r^\infty \frac{y^{-\epsilon}}{(1+y)^2} dy$$

and $r = b/Q^2$.

If $r \geq 1$, then

$$J(r, \epsilon) = \frac{1}{r^\epsilon} \left\{ \frac{1}{1+r} + \frac{\epsilon}{r} \left\{ \ln \left(\frac{1+r}{r} \right) - \frac{1}{1+\epsilon} \right\} - \epsilon(1+\epsilon) \sum_{n=1}^{\infty} \frac{(-1)^{n+1}}{n(n+1+\epsilon)r^{(n+1)}} \right\}. \quad (19)$$

If $r < 1$, then

$$\int_r^{\infty} \frac{y^{-\epsilon}}{(1+y)^2} dy = \frac{\pi\epsilon}{\sin(\pi\epsilon)} - \int_{1/r}^{\infty} \frac{y^\epsilon}{(1+y)^2} dy. \quad (20)$$

Hence

$$J(r, \epsilon) = \frac{\pi\epsilon}{\sin(\pi\epsilon)} - J(1/r, -\epsilon) \quad (21)$$

and the series for $r > 1$ in (19) can be used. These series have two advantages ensuring speed and accuracy of computation:

- the series are alternating so, provided the number of terms is not too large in view of the numerical precision used, the error in the expansion is known and the degree of accuracy easily controllable;
- the expansion variable is the ratio of the integrand lower limit to Q^2 and for many of the points this is sufficiently far from unity for the series to converge adequately after only a few terms. Even for a unit ratio, the convergence is not prohibitively slow.

Acknowledgements

We would like to thank Dr. J. Forshaw for several helpful discussions; and PPARC for financial support.

References

- [1] A.Donnachie and P.V.Landshoff, Phys. Lett. **B296** (1992) 227
- [2] H1 collaboration: I.Abt et al., Nucl. Phys. **B407** (1993) 515
- [3] ZEUS collaboration: M.Derrick et al., Phys. Lett. **B316** (1993) 412
- [4] G.Shaw, Phys. Lett. **B318** (1993) 221
- [5] P.Moseley and G.Shaw, Phys. Rev. **D52** (1995) 4941
- [6] H1 collaboration: S. Aid et al. Nucl. Phys. **B470** (1996) 3
- [7] ZEUS collaboration: M. Derrick et al. Zeit. Phys. **C72** (1996) 399
- [8] E665 collaboration: M. R. Adams et al. Phys. Rev. **D54** (1996) 3006
- [9] V.Del Duca, S.J.Brodsky, and P.Hoyer, Phys. Rev. **D46** (1992) 931
- [10] P.Moseley and G.Shaw, J.Phys.G **21** (1995) 1043
- [11] G.Shaw, Phys.Rev. **D47** (1993) R3676
- [12] G. Shaw, Phys. Lett. **B 226** (1989) 125
- [13] M.Arneodo, Physics Reports **240** (1994) 301
- [14] For a review and references to the early literature on this subject, see A.Donnachie and G.Shaw in ‘Electromagnetic Interactions of Hadrons’, Vol. 2, ed. A.Donnachie and G.Shaw (Plenum, New York, 1978)
- [15] A.Donnachie and P.V.Landshoff, Zeit. Phys. **C61** (1994) 139
- [16] H1 collaboration: paper presented to the International Conference on High Energy Physics, Glasgow 1994
- [17] NMC Collaboration: M. Arneodo et al. Phys. Lett. **B364** (1995) 107
- [18] D. O. Caldwell et al. Phys. Rev. **D7** (1973) 1362
- [19] D. O. Caldwell et al. Phys. Rev. Lett. **40** (1978) 1222
- [20] H1 collaboration: T. Ahmed et al. Phys. Lett. **B299** (1993) 374
- [21] H1 collaboration: S. Aid et al. Zeit. Phys. **C69** (1995) 27
- [22] ZEUS collaboration: M. Derrick et al. Zeit. Phys. **C63** (1994) 391
- [23] H. Fraas, B. J. Read and D. Schildknecht, Nucl. Phys. **B86** (1975) 346

Tables

Data source		Number of points	χ^2
Structure Function data	H1	64	35.7
	ZEUS	47	47.1
	NMC	66	93.9
	E665	77	74.0
Real photo-absorption	Caldwell'73	9	8.8
	Caldwell'78	30	33.8
	HERA	3	2.3
All data		296	295.6

Table 1: Breakdown of χ^2 into contributions from different data sets to the global fit.

Diffractive(pomeron)	
m_0^2	0.466 ± 0.008
α_P	1.059 ± 0.007
A	0.629 ± 0.022
m_J^2	6.28 ± 0.08
α'_P	1.289 ± 0.007
\tilde{A}	0.457 ± 0.019
l_C	17.5 ± 0.3
Non-Diffractive(Regge)	
A_R	0.163 ± 0.029
a_R	0.039 ± 0.009
α_R	0.547(fixed)

Table 2: Parameter values and errors resulting from the global fit. (Natural units, based on the GeV , are used throughout.)

	Omitted Data Set						
	Structure Function				Photoabsorption		
	H1	ZEUS	E665	NMC	Caldwell'73	Caldwell'78	HERA
m_0^2	0.455	0.465	0.463	0.508	0.458	0.463	0.469
α_P	1.054	1.059	1.055	1.067	1.049	1.050	1.064
A	0.628	0.628	0.638	0.655	0.654	0.653	0.617
m_J^2	5.823	6.497	6.303	6.277	5.945	5.911	6.339
α'_P	1.291	1.316	1.290	1.274	1.286	1.287	1.290
\tilde{A}	0.432	0.410	0.454	0.490	0.458	0.455	0.451
l_C	13.48	16.90	17.42	11.60	17.82	17.72	17.32
A_R	0.170	0.164	0.155	0.012	0.137	0.138	0.176
a_R	0.0459	0.0402	0.0392	0.00029	0.0382	0.0334	0.0412
χ^2	259	236	221	188	286	262	293
No. of Points	232	249	219	230	287	266	293

Table 3: Parameter and χ^2 values for fits with one data set in turn excluded.

Figure Captions

Figure 1 Hadronic behaviour of the photon for different values of the coherence length l and invariant mass squared m^2 of the photon fluctuations, where $l = 1/2Mx$ for $m^2 = Q^2$. Here l_C and M_J are the critical values of the coherence length and fluctuation mass that separate the two types of hadronic behaviour. Another critical coherence length $l_0 \approx 1f$ separates the hadronic and purely electromagnetic behaviour.

Figure 2 The hadron dominance model Eq.(4).

Figure 3 The 1994 fits [5] to the 1994 H1 data [16] at $Q^2 = 12 \text{ GeV}^2$, for the values $\alpha'_P = 1.27$ (dashed line) and $\alpha'_P = 1.08$ (solid line).

Figure 4 Comparison of the 1994 fits [5] with the 1996 H1 data [6] at $Q^2 = 12 \text{ GeV}^2$. The curves again correspond to $\alpha'_P = 1.27$ (dashed line) and $\alpha'_P = 1.08$ (solid line).

Figure 5 Comparison of the 1994 fits [5] with the 1996 H1 data [6] at $Q^2 = 1.5$ and 5 GeV^2 for $\alpha'_P = 1.27$ (dashed line).

Figure 6 Comparison of the data from various experiments at $x = 0.0125$ (lower set) and $x = 0.008$ (upper set), where the latter have been scaled by a factor of two, for clarity. The E665 points for $x = 0.008$ have been obtained by linearly interpolating between $x = 0.007$ and 0.009 , and the HERA data have also been interpolated slightly from neighbouring points. The dashed(solid) lines show the result of the global fit described in the text for $x = 0.0125(0.008)$ respectively.

Figure 7 Comparison of the global fit with the 1996 H1 data [6] for representative Q^2 values.

Figure 8 Comparison of the global fit with the 1996 ZEUS data [7].

Figure 9 Comparison of the global fit with the E665 data [8] for representative x -values.

Figure 10 Comparison of the global fit with the NMC data [17].

Figure 11 Comparison of the global fit with the real photoabsorption data [18, 19, 20, 21, 22].

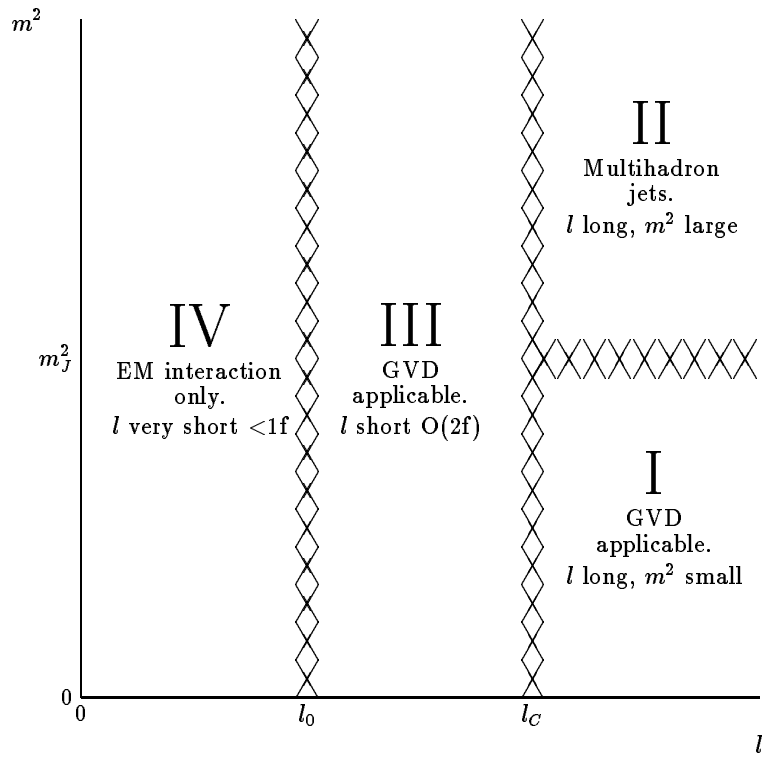


Figure 1: Hadronic behaviour of the photon for different values of the coherence length l and invariant mass squared m^2 of the photon fluctuations, where $l = 1/2Mx$ for $m^2 = Q^2$. Here l_C and M_J are the critical values of the coherence length and fluctuation mass that separate the two types of hadronic behaviour. Another critical coherence length $l_0 \approx 1f$ separates the hadronic and purely electromagnetic behaviour.

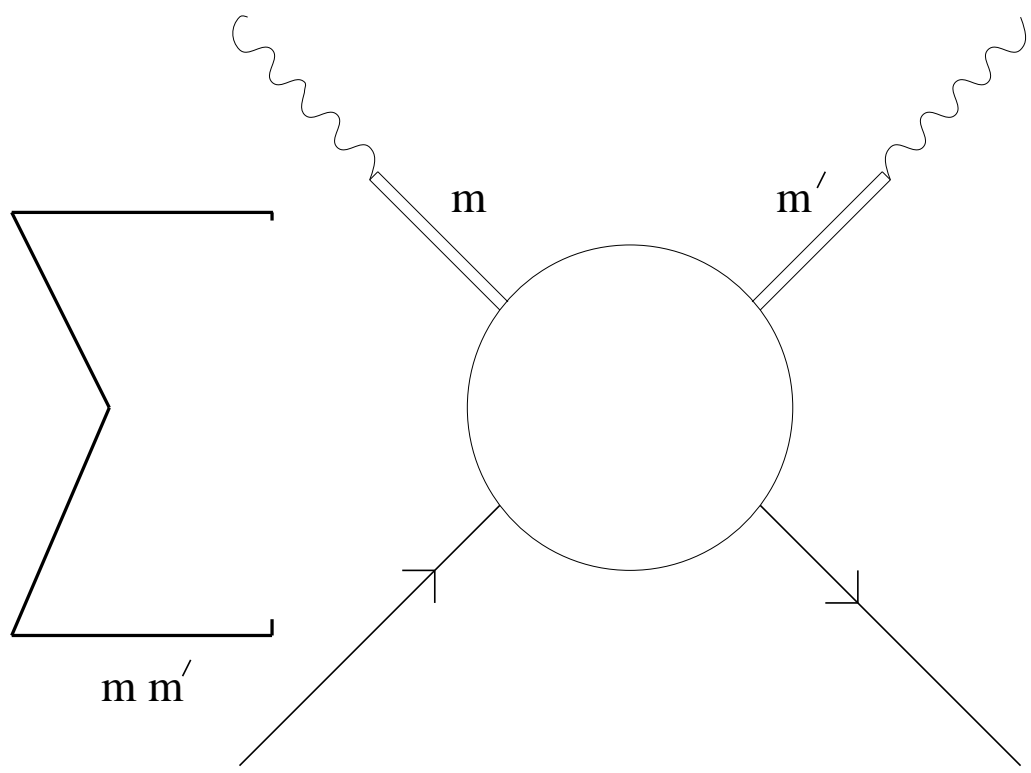


Figure 2: The hadron dominance model (4)

F_2^P

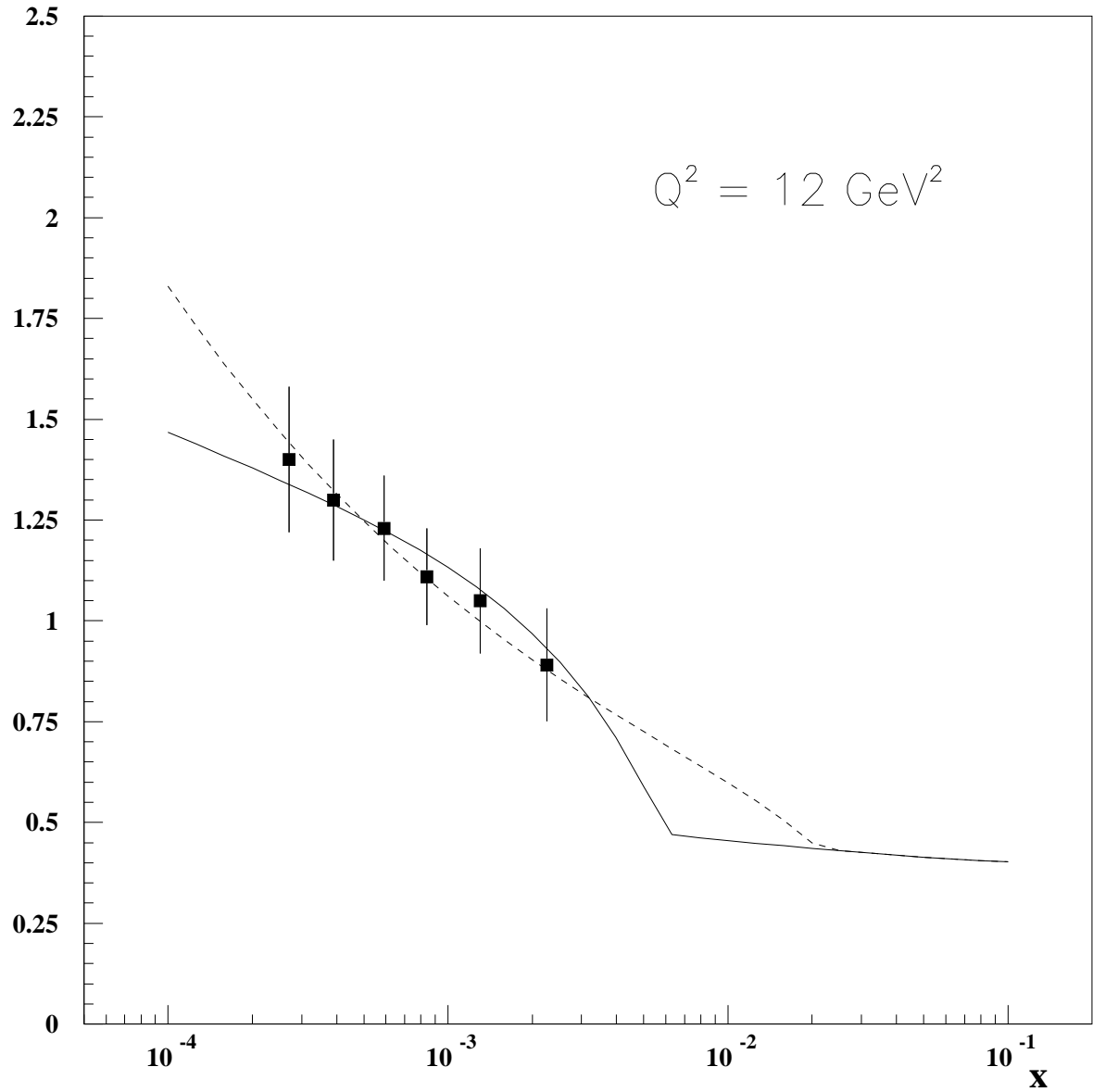


Figure 3: The 1994 fits [5] to the 1994 H1 data [16] at $Q^2 = 12 \text{ GeV}^2$, for the values $\alpha'_P = 1.27$ (dashed line) and $\alpha'_P = 1.08$ (solid line).

F_2^P

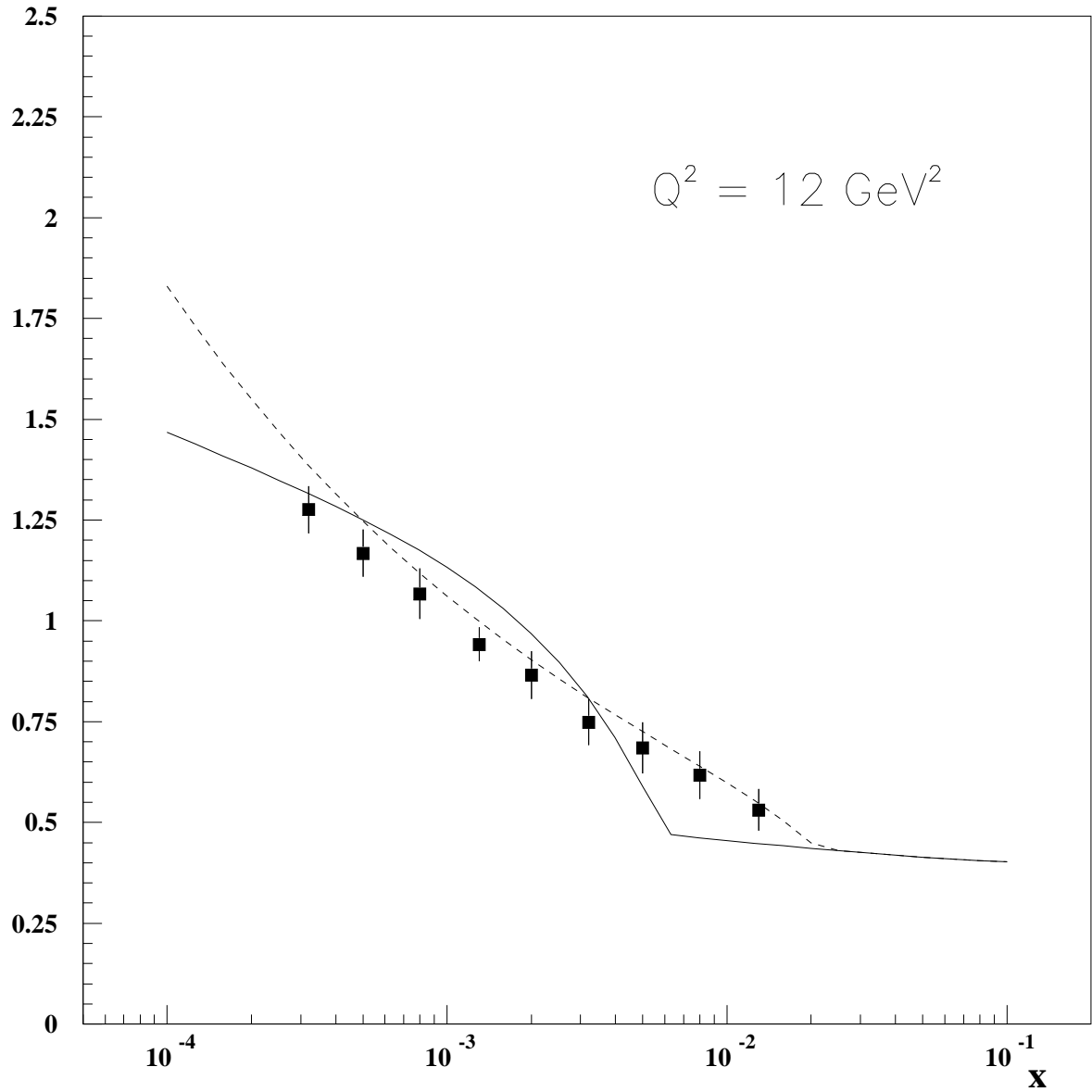


Figure 4: Comparison of the 1994 fits [5] with the 1996 H1 data [6] at $Q^2 = 12 \text{ GeV}^2$. The curves again correspond to $\alpha'_P = 1.27$ (dashed line) and $\alpha'_P = 1.08$ (solid line).

F_2^P

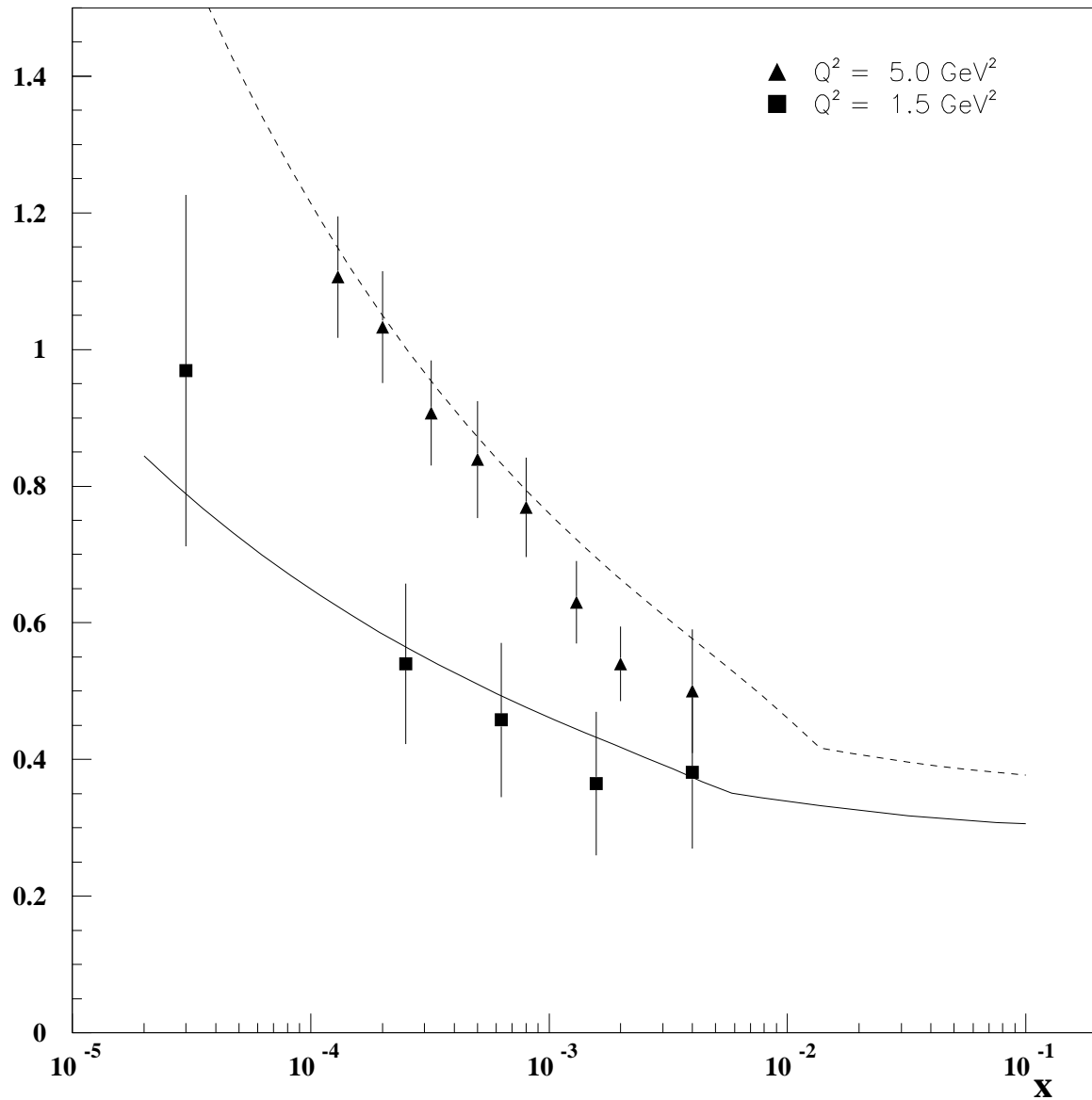


Figure 5: Comparison of the 1994 fits [5] with the 1996 H1 data [6] at $Q^2 = 1.5$ and 5 GeV^2 for $\alpha'_P = 1.27$ (dashed line).

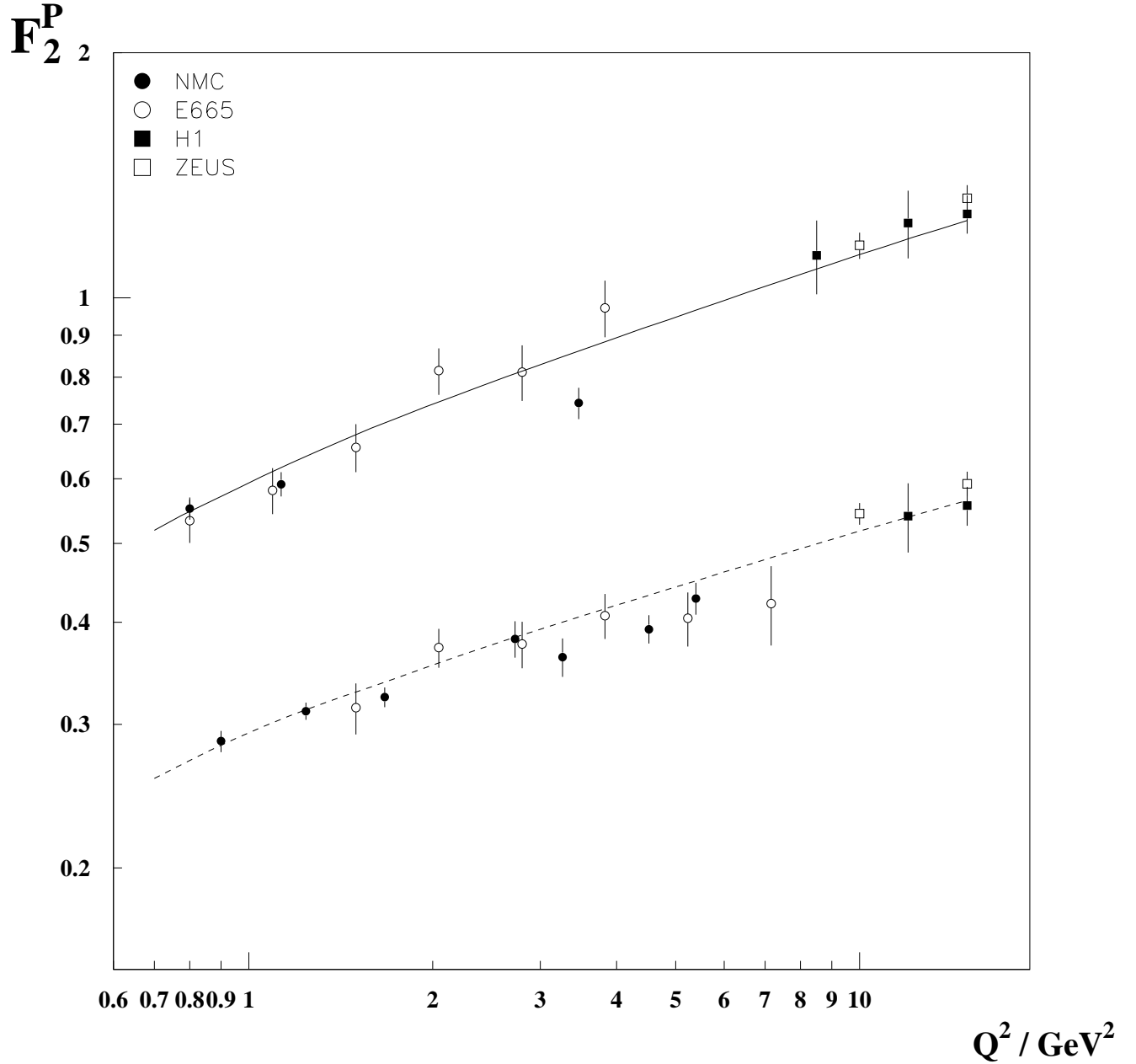


Figure 6: Comparison of the data from various experiments at $x = 0.0125$ (lower set) and $x = 0.008$ (upper set), where the latter have been scaled by a factor of two, for clarity. The E665 points for $x = 0.008$ have been obtained by linearly interpolating between $x = 0.007$ and 0.009 , and the HERA data have also been interpolated slightly from neighbouring points. The dashed (solid) lines show the result of the global fit described in the text for $x = 0.0125$ (0.008) respectively

F_2^P

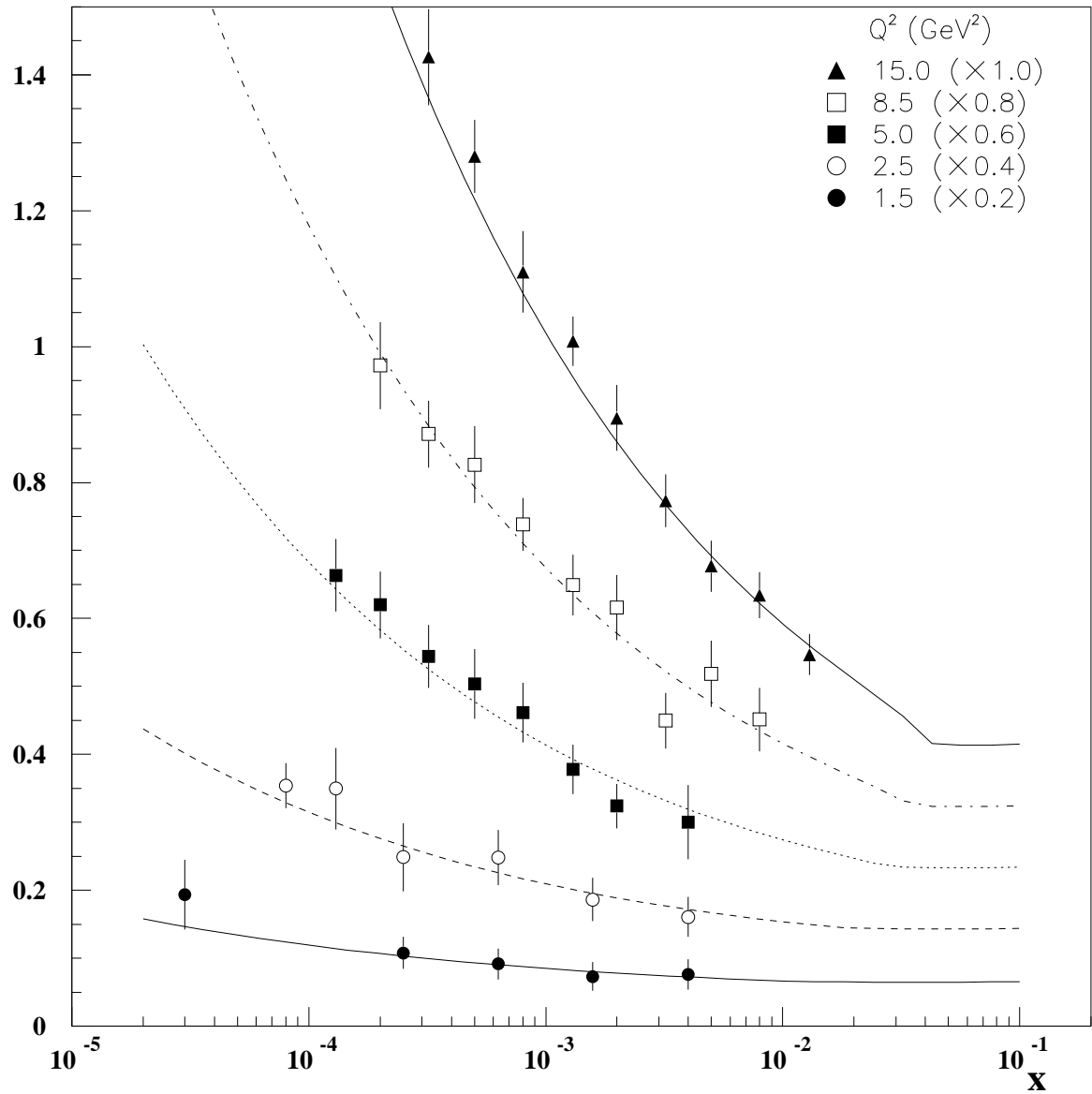


Figure 7: Comparison of the global fit with the 1996 H1 data [6] for representative Q^2 values.

F_2^P

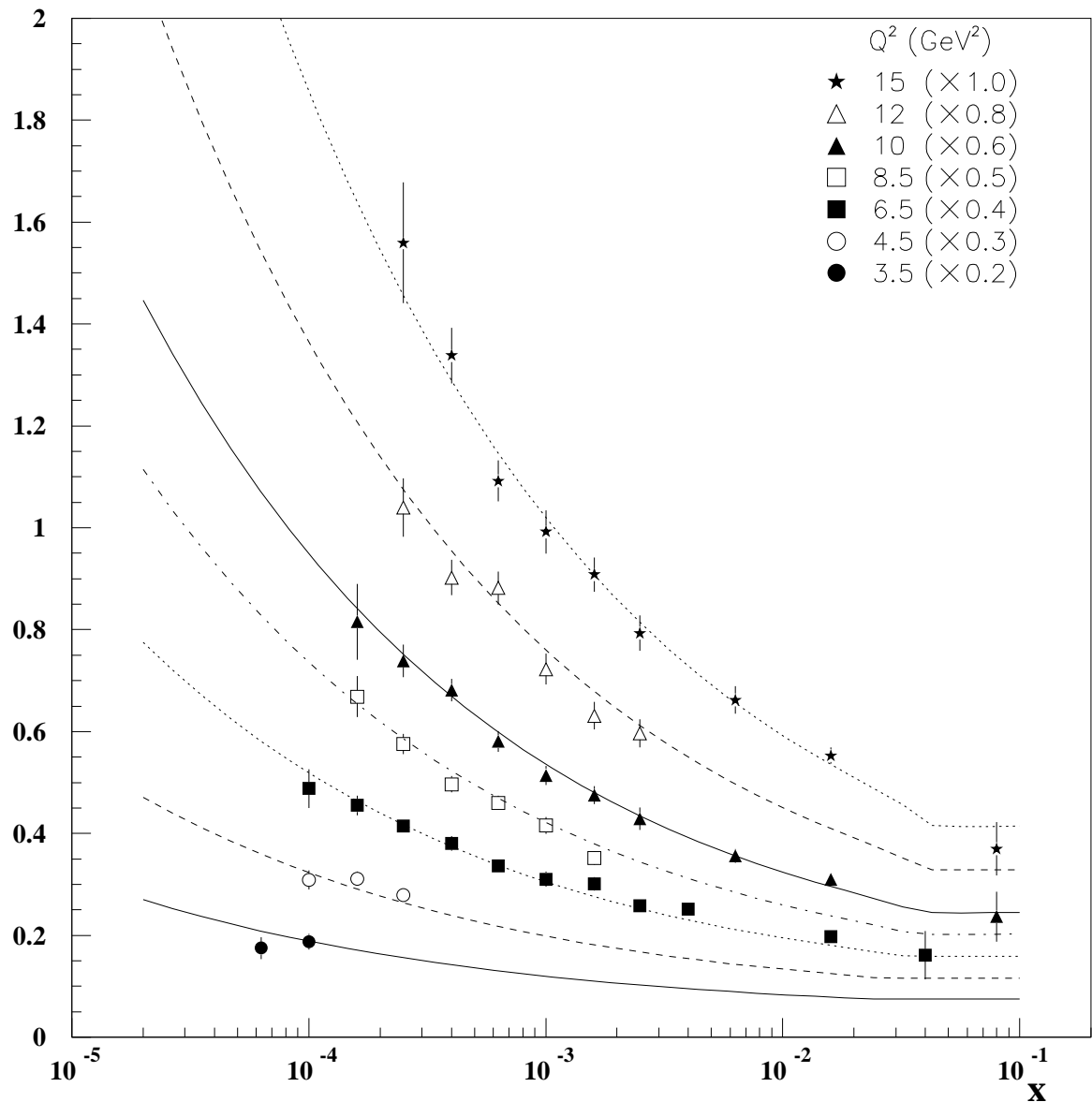


Figure 8: Comparison of the global fit with the 1996 ZEUS data [7].

F_2^P

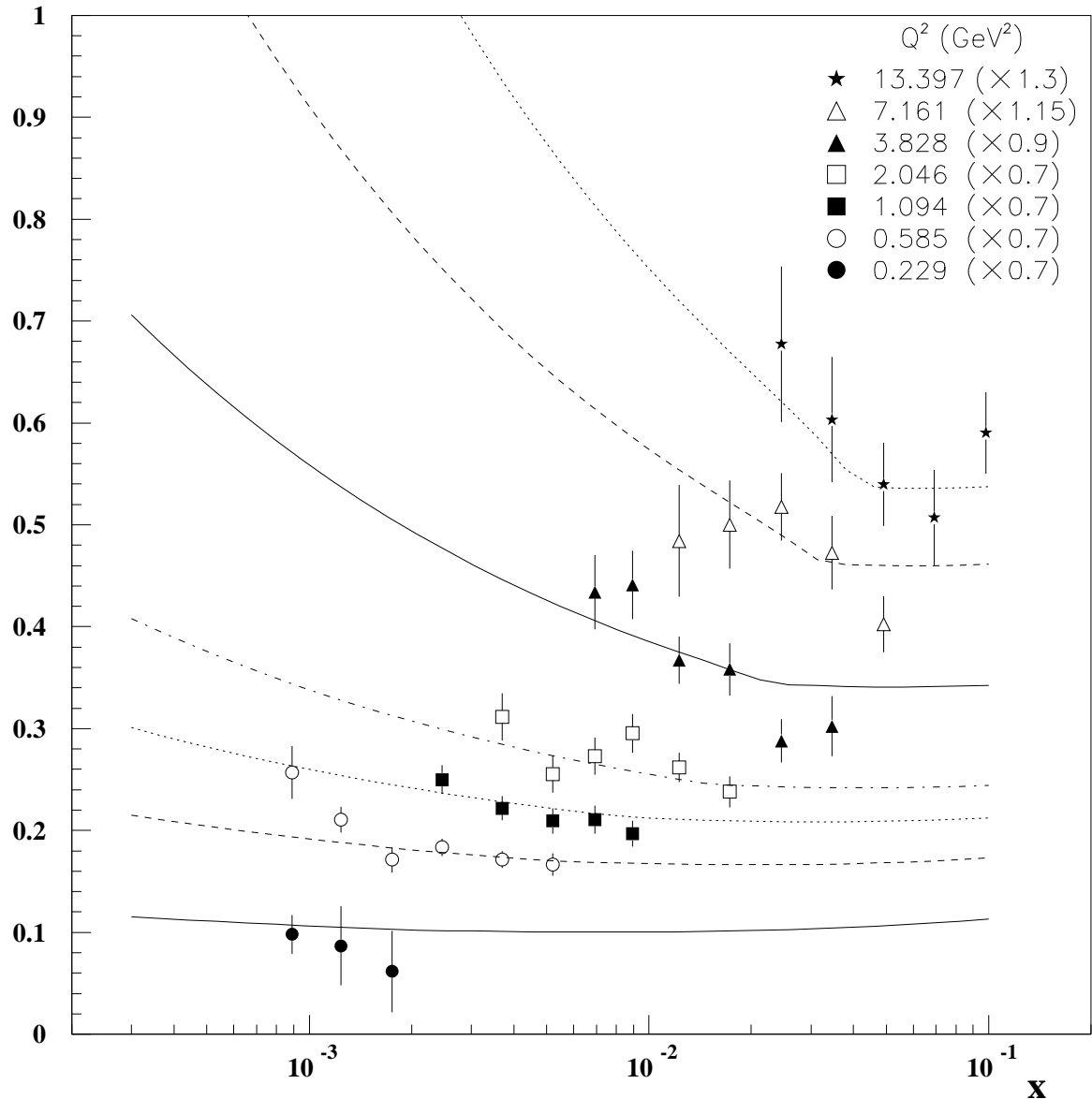


Figure 9: Comparison of the global fit with the E665 data [8] for representative x -values.

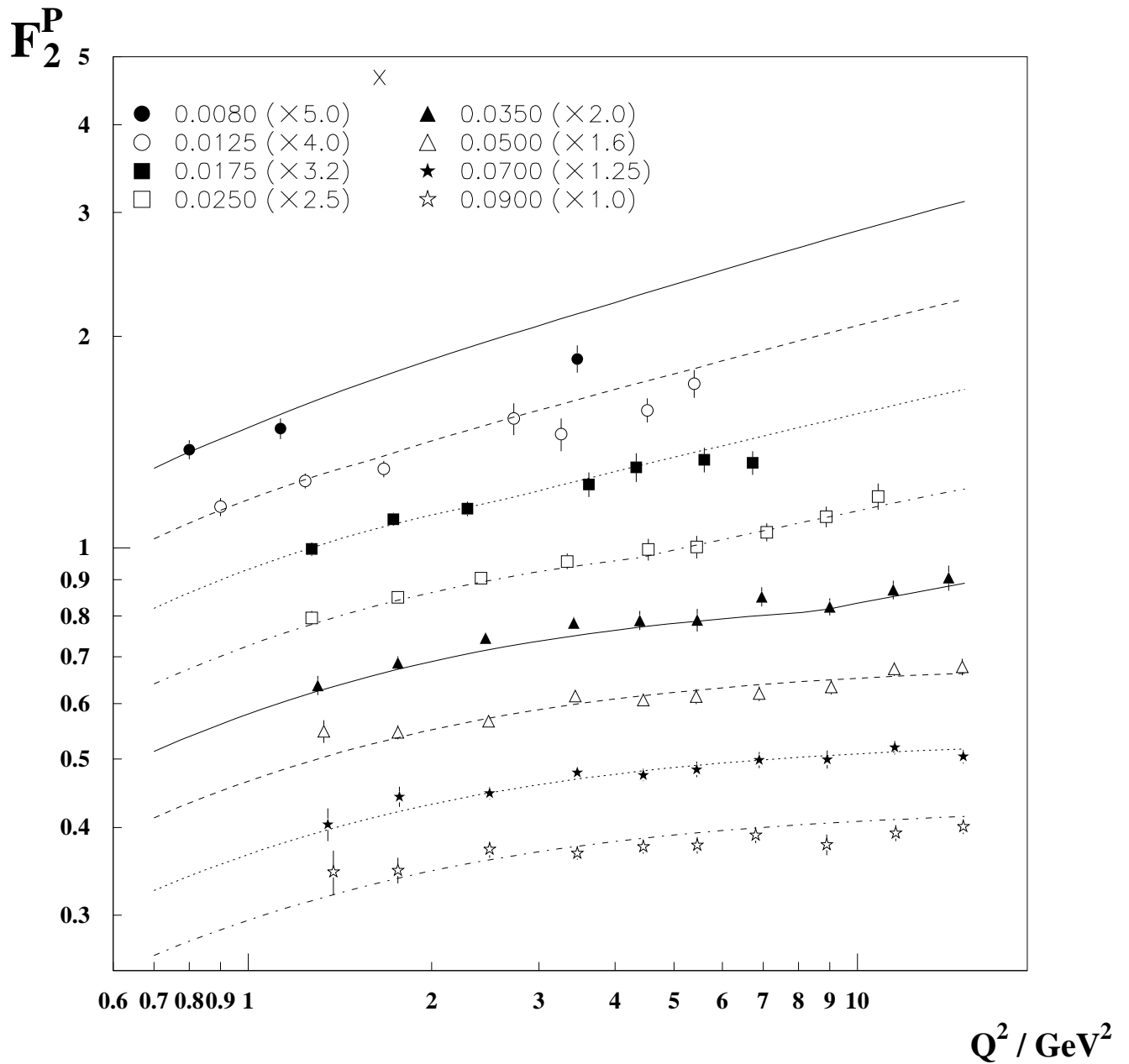


Figure 10: Comparison of the global fit with the NMC data [17].

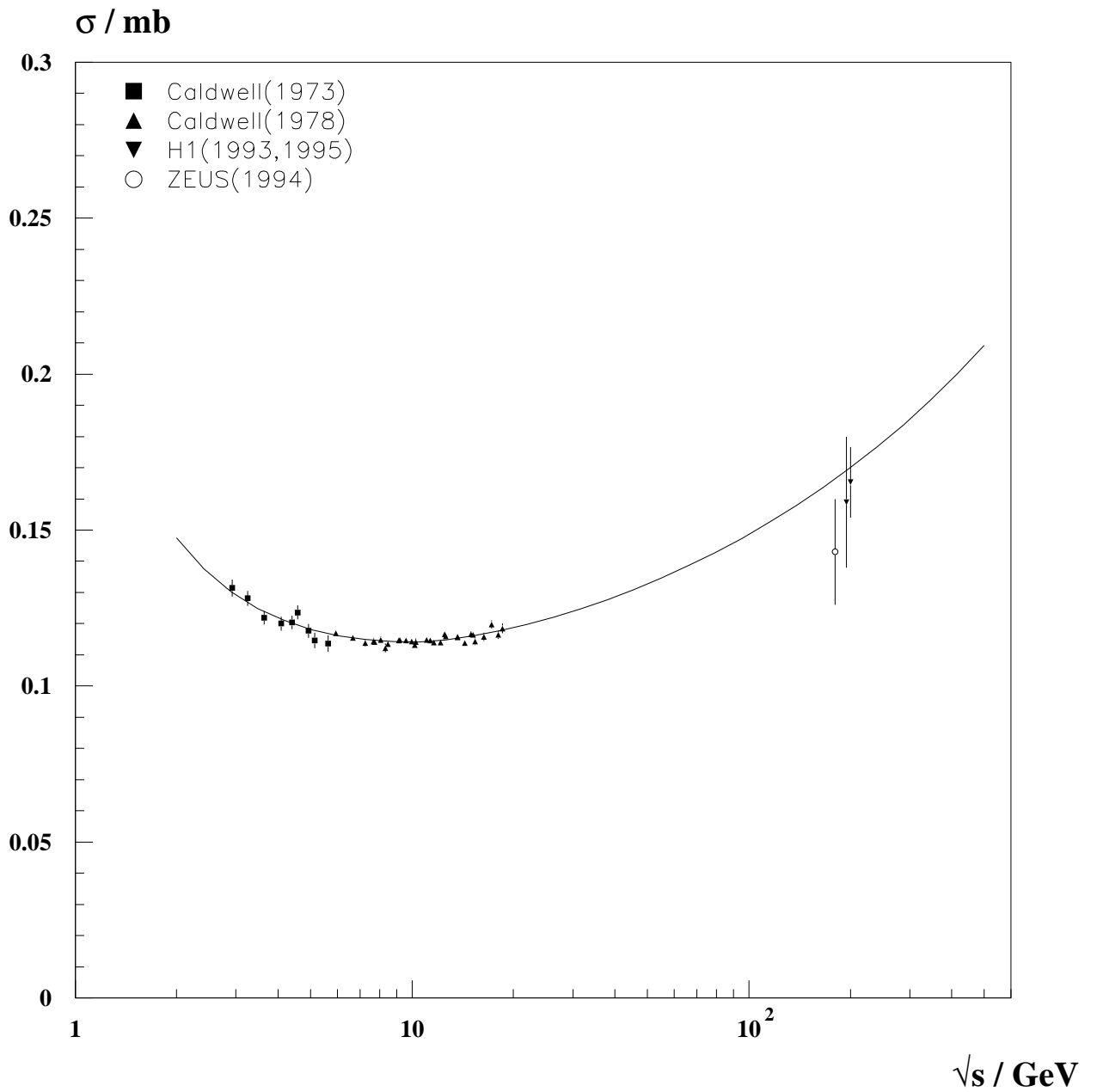


Figure 11: Comparison of the global fit with the real photoabsorption data [18, 19, 20, 21, 22].